Dynamical decoupling noise spectroscopy

Gonzalo A. Álvarez* and Dieter Suter†
Fakultät Physik, Technische Universität Dortmund, Dortmund, Germany.

Decoherence is one of the most important obstacles that must be overcome in quantum information processing. It depends on the qubit-environment coupling strength, but also on the spectral composition of the noise generated by the environment. If the spectral density is known, fighting the effect of decoherence can be made more effective. Applying sequences of inversion pulses to the qubit system, we generate effective filter functions that probe the environmental spectral density. Comparing different pulse sequences, we recover the complete spectral density function and distinguish different contributions to the overall decoherence.

PACS numbers: 03.65.Yz, 76.60.Es, 76.60.Lz, 03.67.Pp

Introduction.— Quantum information processing relies on the robust control of quantum systems. A quantum system is always influenced by external degrees of freedom, the environment, that disturb the quantum information by a process called decoherence [1]. Many strategies were developed to fight this degradation of information. These methods are based on correction of errors [2, 3] and decoupling the environment [4–7]. Fighting decoherence successfully requires knowledge of the noise spectral density to design suitable quantum processes [8–11].

Within the decoupling methods, one simple strategy is called dynamical decoupling (DD) [7, 12]. It is based on the application of a sequence of control pulses to the system to effectively isolate it from the environment. Different DD sequences were developed [7, 12–14] and tested experimentally [15–20]. Different sources modify the performance of DD sequences. Once pulse errors are small, the spectral density of the system-environment (SE) interaction becomes the main factor [8, 14, 15, 19, 21–24]. Consequently a DD sequence has to be judiciously designed according to the particular noise spectral density to be decoupled [14, 15, 21–24].

In this paper, we present a method to determine the spectral density of the SE interaction. The method is based on previous results that the decay rate of a qubit during DD is given by the overlap of the bath spectral density function and a filter function generated by the DD sequence [14, 15, 19, 21–24]. The filter function is given by the Fourier transform of the SE interaction modified by the control pulses: each π-pulse changes the sign of the SE coupling. When many DD cycles are applied to the system, the filter functions become a sum of $\delta-$functions [19]. Consequently, the decoherence time is given by a discrete sum of spectral densities. A judicious choice of the DD sequence thus allows one to probe the environmental spectral density at selected frequencies. Combining several measurements, it is possible to obtain a detailed picture of the noise spectral distribution.

A qubit as the noise probe.— We consider a single qubit $\hat{S}$ as the probe. It is coupled to the bath to be studied with a purely dephasing interaction. In a resonantly rotating frame of reference [6], the free evolution Hamiltonian is $\widehat{\mathcal{H}}_f = \widehat{\mathcal{H}}_{SE} + \widehat{\mathcal{H}}_E$, where $\widehat{\mathcal{H}}_E$ is the environment Hamiltonian and $\widehat{\mathcal{H}}_{SE} = b_{SE}\hat{S}_z\hat{E}$, is a general pure dephasing system-environment (SE) interaction. $\hat{E}$ is some operator of the environment and b_{SE} the SE coupling strength. This type of interaction is encountered in a wide range of solid-state spin systems, as for example nuclear spin systems in NMR [4, 5, 17, 19], electron spins in diamonds [18], electron spins in quantum dots [25], donors in silicon [26], etc.

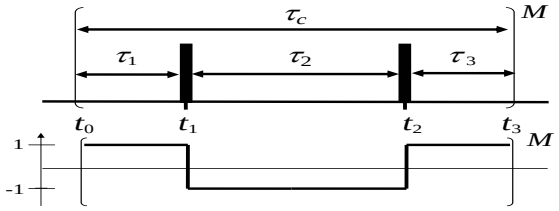

Figure 1: The top panel shows a two pulse sequence with M repetitions of the cycle (duration τ_c) and the bottom panel the resulting modulating function f.

We consider the application of a sequence of short, strong pulses that invert the probe qubit [7, 12]. As shown in Fig. 1, we assume N instantaneous pulses at times t_i, with delays $\tau_i = t_i - t_{i-1}$ between the pulses for $i = 2, .., N+1$ and $\tau_1 = t_1 - t_0$, where $t_0 = 0$ and $t_{N+1} = \tau_c$.

While such a sequence can refocus a static system-environment interaction completely, any time-dependence reduces its efficiency. We calculate the remaining decay rate for the case where the environment can be well described by a stochastic noise. This results are also valid for a quantum second order approximation of the time-dependent SE interaction [6]. We now eliminate the environment-Hamiltonian $\widehat{\mathcal{H}}_E$ by using an interaction representation with respect to the evolution of the isolated environment. The system-environment Hamiltonian then becomes

$$\widehat{\mathcal{H}}_{SE}^{(E)}(t) = b_{SE}\hat{S}_z e^{-i\widehat{\mathcal{H}}_E t}\hat{E}e^{i\widehat{\mathcal{H}}_E t}. \qquad (1)$$

Since $\widehat{\mathcal{H}}_E$ does not commute with $\widehat{\mathcal{H}}_{SE}$, the effective

system-environment interaction $\widehat{\mathcal{H}}_{SE}^{(E)}$ is time-dependent and the system experiences a fluctuating coupling with the environment.Tracing over the bath variables replaces $b_{SE}e^{-i\widehat{\mathcal{H}}_E t}\hat{E}e^{i\widehat{\mathcal{H}}_E t}$ by the stochastic function $b_{SE}E(t)$. For simplicity we assume that this random field has a Gaussian distribution with zero average, $\langle E(t)\rangle = 0$. The autocorrelation function is $\langle E(t)E(t+\tau)\rangle = g(\tau)$ and the spectral density $S(\omega)$ of the system-bath interaction is the Fourier transform of $b_{SE}^2 g(\tau)$.

The free evolution operator for a given realization of the random noise is $\exp\left\{-i\phi(t)\hat{S}_z\right\}$, where $\phi(t) = b_{SE}\int_0^t dt_1 E(t_1)$ is the phase accumulated by the probe spin during the evolution. Considering now the effect of the pulses, they generate reversals of $\widehat{\mathcal{H}}_{SE}(t)$. If the pulses are applied during the interval τ_c as described above, the accumulated phase after M cycles $\phi(M\tau_c)$ becomes $\phi(M\tau_c) = b_{SE}\int_0^{M\tau_c} dt' f_N(t', M\tau_c)E(t')$, where the modulating function $f_N(\tau', M\tau_c)$ switches between ± 1 at the position of every pulse [21]. This is depicted in Fig. 1. It was shown that if the initial state of the probe spin is $\hat{\rho}_0 = \hat{S}_{x,y}$, its normalized magnetization under the effects of DD taking the average over the random fluctuations is $\langle s_{x,y}(t)\rangle = e^{-\frac{1}{2}\langle\phi^2(t)\rangle}$, and its decay can be quantified by the exponential's argument $\frac{1}{2}\langle\phi^2(t)\rangle$

$$R(t)t = \frac{\sqrt{2\pi}}{2}\int_{-\infty}^{\infty} d\omega S(\omega)\left|F_N(\omega, M\tau_c)\right|^2, \quad (2)$$

where $F_N(\omega, M\tau_c)$ is the Fourier transform of $f_N(t', M\tau_c)$ [21]. The decay function $R(t)t$ is thus equal to the product of the spectral density $S(\omega)$ of the system-environment coupling and the filter transfer function $F_N(\omega, M\tau_c)$. Examples of this filter function are shown in Fig. 2a for a CPMG sequence ($\tau_2 = 2\tau_1 = 2\tau_3 = \tau$) [4, 5] with $M = 1$ and $M = 40$. We have recently shown that considering the infinite extension of the modulating function, $f_N(t', \infty)$, by a convolution this provides a $F_N(\omega, M\tau_c)$ that is a sum of sinc functions centered at the harmonic frequencies $k\omega_0 = 2\pi k/\tau_c$ of the Fourier series of $f_N(t', \infty)$ [19]. As schematized in Fig. 2a, the maxima of the filter function $|F_N(\omega, M\tau_c)|$ at $\omega = 2\pi k/\tau_c$ have amplitudes given by the filter function $F_N(\omega, \tau_c)$ of a single cycle. Between two harmonics are $(M-2)$ secondary maxima. Their amplitudes with respect to the relevant harmonic fall off $\propto M^{-1}$ [19]. Hence for $t = M\tau_c \gg \tau_B$, the filter function $|F_N(\omega, \tau_M)|$ becomes an almost discrete spectrum given by the Fourier transform of $f_N(t', \infty)$, i.e. $F(\omega, t)$ is represented by a series of δ-functions centered at $k\omega_0$ neglecting the contributions from the secondary maxima [In Eq. (2), $|F_N|^2$ appears]. This is shown by the circles in Fig. 2a. Thus, the decay is exponential with a constant rate

$$R = \sum_{k=1}^{\infty} A_k^2 S(k\omega_0), \quad (3)$$

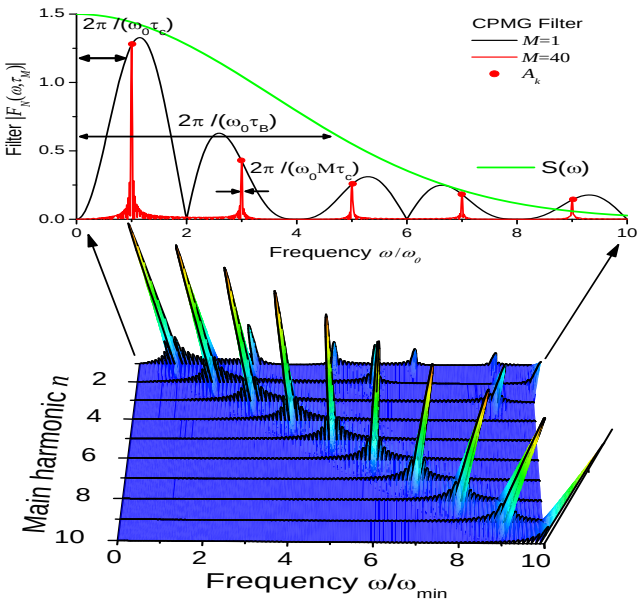

Figure 2: (Color online) (a) The filter function of a CPMG sequence for $M = 1$ (black curve) and $M = 40$ (red curve). The green line shows a Gaussian spectral density which can be probe at the DD harmonics frequencies marked by circles. (b) Filter functions for CPMG sequences with different pulse delays $\tau = 2\pi/(n\omega_{min})$.

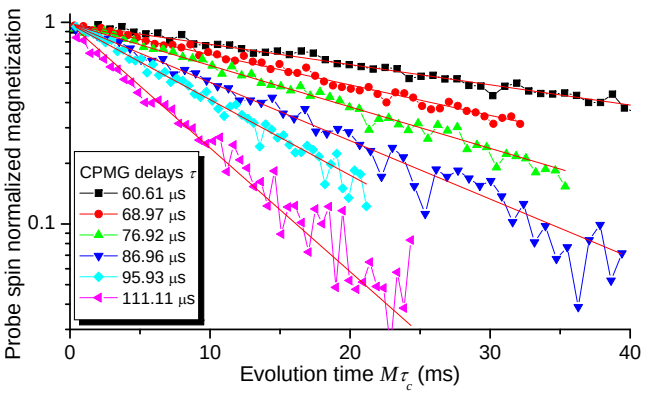

Figure 3: (Color online) Experimental signal decays of the probe spin as a function of the evolution time under CPMG dynamical decoupling. Different curves correspond to different pulse delays. The straight lines represent exponential fits.

with $A_k^2 = \frac{\sqrt{2\pi}}{\tau_c^2}\left|F_N(k\omega_0, \tau_c)\right|^2$, where for a CPMG sequence $A_k \propto 1/k$ for odd k and 0 otherwise. This is the basis for the DD noise spectroscopy methodology presented in this letter. Examples of the probe spin signal decay are shown in Fig. 3.

Noise spectroscopy.— Assuming for the moment that the sum in Eq. (3) collapses to the $k = 1$ term, we can clearly trace out the bath spectral density by varying the delay between the pulses [10]. However, for real DD sequences, we always have an infinite series, where all harmonics con-

tribute to the decay rate with the weight A_k. Determining the spectral density function therefore requires the inversion of Eq. (3). The main difficulty here is that a single measurement depends on an infinite number of unknown spectral density values. We solve this problem by a two-step procedure: in the first step, we combine m measurements with different pulse delays, which we choose such that they probe the spectral density function at a discrete set of harmonic frequencies with different sensitivity amplitudes A_k. In this step, we neglect contributions from the tail of $S(\omega > m\omega_{min})$. This yields a square matrix that we can invert to obtain the values of $S(j\omega_{min})$, $j = 1..m$. From the resulting spectral density function, we estimate a functional form for the tail of the distribution and correct the data for the contributions from the tail. Inverting the matrix again, with the corrected values, gives the final spectral density distribution.

A natural choice for the probing sequence is the CPMG or equidistant sequence, which has harmonics at frequencies $\omega_0 = \pi/\tau$ (circles in Fig. 2a). To simplify inverting equation (3), we choose the pulse delays in the different measurements such that all relevant frequencies, including all harmonics, are multiples of a minimal frequency ω_{min}. We therefore start with a maximum delay $\tau_{max} = \pi/\omega_{min}$, which determines the frequency resolution with which we probe the spectral density function. If the maximum frequency at which we want to probe the spectral density function directly is $m\omega_{min}$, then we need to apply sequences with delays $\tau_n = \tau_{max}/n = \tau_{min}m/n$. Figure 2b shows the relevant filter functions for the first ten sequences. If we neglect the contribution from frequencies $> m\omega_{min}$, the relaxation rates R_n for the different experiments are given by a system of m linear equations

$$R_n = \sum_{k=1}^{[m/n]} A_k^2 S(nk\omega_{min}) = \sum_{j=1}^{m} U_{nj} S_j, \qquad (4)$$

where $[m/n]$ denotes the integer part of m/n and $j = nk$. The elements A_k^2 form an upper triangular matrix $U_{nj} = \sum_{k=1}^{[m/n]} A_k^2 \delta_{j,nk}$, and $S_j = S(j\omega_{min})$ represent the unknown spectral density values, which can formally be calculated as $S_j = \sum_{n=1}^{m} (U^{-1})_{jn} R_n$

We now correct for the omitted contributions from the high-frequency tail of the infinite sum by approximating it with a suitable functional form, which depends on the system being studied. Typical examples include a power law decay, lorentzian or gaussian decay, or a sudden cut off like in an ohmic bath. In the system that we used as an example (see below), the experimental data can be approximated very well by a power law dependence, as shown in Fig. 4.

If the tail satisfies a power law $S_j = \frac{C}{j^\alpha}$ for $j > n_p$, then

$$R_{n>n_p} = \sum_{k=1}^{\infty} \frac{A_k^2 C}{(nk)^\alpha} = \frac{C}{n^\alpha} \sum_{k=1}^{\infty} \frac{A_k^2}{k^\alpha} = \frac{C\Lambda_\alpha}{n^\alpha}. \qquad (5)$$

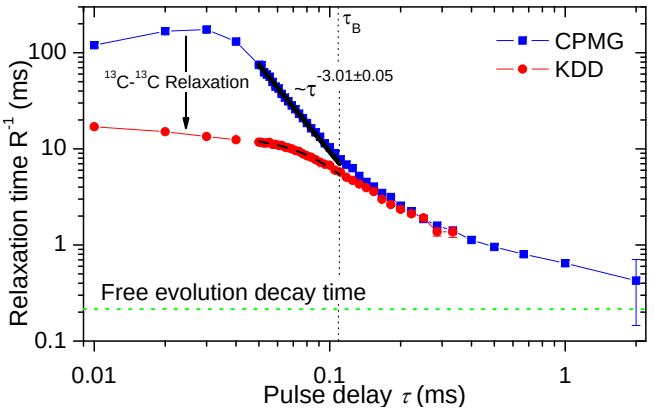

Figure 4: (Color online) Experimental relaxation times of the probe spin under the application of CPMG (blue squares) and KDD (red circles) sequences. The black solid line represents a power law fitting to the CPMG data and the green dotted line the asymptotic free evolution decay rate. The black dashed line is a fitting to the KDD data with an expression $(R_{13C} + C'\tau^\alpha)^{-1}$, where $\alpha = 3.0 \pm 0.1$ and $R_{13C} = (74 \pm 1)\ \mu s^{-1}$ represents the ^{13}C-^{13}C relaxation rate.

This relation is represented by the black solid line in Fig. 4. We can now modify Eq. (4) adding the neglected terms and then the relaxation rates satisfy

$$R_n = \sum_{j=1}^{m} U_{nj} S_j + \left(\frac{\Lambda_\alpha C}{n^\alpha} - \sum_{j=1}^{m} U_{nj} \frac{C}{j^\alpha} \right),$$

where $\left(\frac{\Lambda_\alpha C}{n^\alpha} - \sum_{j=1}^{m} U_{nj} \frac{C}{j^\alpha} \right) = \frac{C}{n^\alpha} \sum_{k>m-n+1} \frac{A_k^2}{k^\alpha}$ represents the effective spectral density summing the contribution from all harmonics $k > m - n + 1$. The spectral density is now determined from $S_j = \sum_{n=1}^{m} (U^{-1})_{jn} \left(R_n - \frac{\Lambda_\alpha C}{n^\alpha} \right) + \frac{C}{j^\alpha}$.

Experimental determination of $S(\omega)$.— For the experimental test, we chose ^{13}C nuclear spins ($S = 1/2$) as probe qubits. We used polycrystalline adamantane where the carbon nuclear spins are coupled to an environment of ^{1}H nuclear spins ($I = 1/2$) that act as a spin-bath. The natural abundance of the ^{13}C nuclei is about 1%, and to a good approximation each ^{13}C nuclear spin is surrounded by about 150 ^{1}H nuclear spins. The interaction with the environment is thus dominated by the ^{13}C-^{1}H magnetic dipole coupling [6]. To determine the bath spectral density we applied the equidistant sequences CPMG and KDD [20] to the probe spin for different delays between pulses $\tau_n = \tau_{max}/n$, with $n = 1..40$ and $\tau_{max} = 2$ms. For CPMG, we chose an initial state longitudinal to the pulses because then pulse error effects can be neglected [5, 17]. Figure 3 shows examples of the ^{13}C signal decays. The lines in the figure show the fitted exponential decays, which agree very well with the data points in this range. This demonstrates that we are in the regime where the filter functions are discrete. KDD was shown to be robust against pulse errors,

independent of the initial condition [20]. For ideal pulses, both sequences have the same filter function. As shown in Fig. 4 the observed relaxation times for this system depend on the pulse spacing like $\propto \tau^{-3}$ for the CPMG sequence over the range $\tau = [50\,\mu s, 110\,\mu s]$. We only used the data points for $\tau > 50\,\mu$s to determine the parameters C and α, since Fig. 4 indicates that other processes contribute to the relaxation at shorter delays. From the fitting process, we found $\alpha = 3.01 \pm 0.05$ and $\Lambda_\alpha \approx 1.004$. Thus, the contribution of the infinite series is only $4 \cdot 10^{-3}$ and thus almost negligible. Figure 4 also shows that the dependence of the decoherence rates changes at $\tau \gtrsim 100\,\mu$s. This agrees with the value that we determined earlier for the correlation time of the bath [17].

We observe in the KDD case that the relaxation time saturates for τ shorter than $50\,\mu$s and in general is lower than the CPMG cases (Fig. 4). This difference can be attributed to the effect of ^{13}C-^{13}C couplings. Because in the CPMG sequence all pulses generate the same rotation, the overall effect of the pulse cycle is to first order equivalent to a constant effective field, which stabilizes the observable magnetization against the effect of ^{13}C-^{13}C couplings [27]. In the KDD case, the state is not longitudinal to the pulses and no spin-lock effect is observed. The saturation of the relaxation time for the CPMG case for $\tau < 50\,\mu$s can be attributed to the finite rf field strength or, equivalently, to the finite duration of the pulses. Pulse errors may also contribute in this regime.

Because in the KDD case, the ^{13}C-^{13}C interaction eclipses the spectral density of the proton bath, assuming a ^{13}C-^{13}C relaxation rate independent of the pulse delays we fit an expression $(R_{13\mathrm{C}} + C'\tau^\alpha)^{-1}$ over the range $[50\,\mu s, 110\,\mu s]$ where the CPMG data behave as a power law (dashed line in Fig 4). We obtained $R_{13\mathrm{C}} = (74 \pm 1)\ \mu\mathrm{s}^{-1}$ for the ^{13}C-^{13}C relaxation rate and $\alpha = 3.0 \pm 0.1$ which perfectly matches with the CPMG result. If we subtract the $R_{13\mathrm{C}}$ contribution, we obtain the spectral density represented by the empty circles in Fig. 5, which are almost identical to the result obtained with the CPMG sequence (solid squares). For shorter τ in the KDD case, the relaxation time starts to increase faster because of the effective spin lock generated by the composite Knill pulses that constitute the KDD sequence [20].

Conclusions.— We have developed a method to determine the noise spectral density generated by a bath. It is based on modulating the system-environment interaction by applying sequences of inversion pulses to the system. If the sequence consists of many repetitions of a basic cycle, the resulting decays are exponentials and the decay rates are given by the spectral density at discrete frequencies. This allows one to build a linear system of equations that can be inverted to obtain the unknown spectral density function. We applied the method to obtain the spectral density of the ^{13}C- ^{1}H interaction in adamantane. Applying this method to other systems will help fighting decoherence, e.g. by optimizing DD sequences by reducing the overlap of their filter functions with the noise spectral density [14, 15, 21–24].

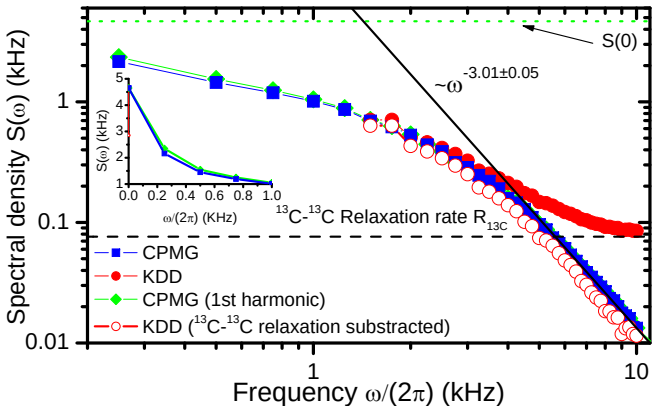

Figure 5: (Color online) Experimentally determined noise spectral density. The inset shows in a linear scale the low frequency regime. The green dotted line represents the free evolution decay rate of the probe spin, i.e. $S(0)$.

Acknowledgments.— This work is supported by the DFG through Su 192/24-1. GAA thanks financial support from the Alexander von Humboldt Foundation in the initial stage of this project. We thank Alexandre M. Souza for helpful discussions.

* galvarez@e3.physik.uni-dortmund.de
† Dieter.Suter@tu-dortmund.de

[1] W. H. Zurek, Rev. Mod. Phys. **75**, 715 (2003).
[2] J. Preskill, Proc. R. Soc. Lond. A **454**, 385 (1998).
[3] E. Knill, Nature **434**, 39 (2005).
[4] H. Y. Carr and E. M. Purcell, Phys. Rev. **94**, 630 (1954).
[5] S. Meiboom and D. Gill, Rev. Sci. Instrum. **29**, 688 (1958).
[6] A. Abragam, *Principles of Nuclear Magnetism* (Oxford University Press, London, 1961).
[7] L. Viola, E. Knill, and S. Lloyd, Phys. Rev. Lett. **82**, 2417 (1999).
[8] J. Zhang, X. Peng, N. Rajendran, and D. Suter, Phys. Rev. A **75**, 042314 (2007).
[9] D. D. Bhaktavatsala Rao and G. Kurizki, Phys. Rev. A **83**, 032105 (2011).
[10] J. Bylander, *et al.*, arXiv:1101.4707 (2011).
[11] I. Almog, *et al.*, arXiv:1103.1104 (2011).
[12] W. Yang, Z. Wang, and R. Liu, Front. Phys. **6**, 2 (2010).
[13] K. Khodjasteh and D. A. Lidar, Phys. Rev. Lett. **95**, 180501 (2005).
[14] G. S. Uhrig, New J. Phys. **10**, 083024 (2008).
[15] M. J. Biercuk, *et al.*, Nature **458**, 996 (2009).
[16] J. Du, *et al.*, Nature **461**, 1265 (2009).
[17] G. A. Álvarez, A. Ajoy, X. Peng, and D. Suter, Phys. Rev. A **82**, 042306 (2010).
[18] C. A. Ryan, J. S. Hodges, and D. G. Cory, Phys. Rev. Lett. **105**, 200402 (2010).
[19] A. Ajoy, G. A. Álvarez, and D. Suter, Phys. Rev. A **83**,

032303 (2011).
[20] A. M. Souza, G. A. Álvarez, and D. Suter, Phys. Rev. Lett. **106**, 240501 (2011).
[21] L. Cywinski, R. M. Lutchyn, C. P. Nave, and S. DasSarma, Phys. Rev. B **77**, 174509 (2008).
[22] G. Gordon, G. Kurizki, and D. A. Lidar, Phys. Rev. Lett. **101**, 010403 (2008).
[23] H. Uys, M. J. Biercuk, and J. J. Bollinger, Phys. Rev. Lett. **103**, 040501 (2009).
[24] J. Clausen, G. Bensky, and G. Kurizki, Phys. Rev. Lett. **104**, 040401 (2010).
[25] R. Hanson, *et al.*, Rev. Mod. Phys. **79**, 1217 (2007).
[26] B. E. Kane, Nature **393**, 133 (1998).
[27] G. E. Santyr, R. M. Henkelman, and M. J. Bronskill, J. Magn. Reson. **79**, 28 (1988).